Chemical control of dissolution-driven convection in partially miscible systems: Nonlinear simulations and experiments

Chemical control of dissolution-driven convection in partially miscible systems: nonlinear simulations and experiments

M.A. Budroni *

C. Thomas †, A. De Wit ‡

January 17, 2017

Abstract

Chemical reactions can impact mixing in partially miscible stratifications by affecting buoyancy-driven convection developing when one phase dissolves into the other in the gravity field. By means of combined nonlinear simulations and experiments, we explore the power of an A+B→C type of reaction to either enhance or refrain convective dissolution with respect to the nonreactive system depending on the relative contribution to density of the dissolving species A, of the reactant B initially dissolved in the host phase and of the product C. Nonlinear simulations are performed by solving reaction-diffusion-convection equations describing the dissolution and reactive dynamics when a less dense phase of A is layered on top of a reactive denser solution of B, in which A is partially miscible with a given solubility. The spatio-temporal dynamics and convective patterns observed in the numerical study compare favorably with experiments carried out with (*i*) a liquid alkyl-formate stratified on top of an aqueous solution in which the ester dissolves

*Université libre de Bruxelles (ULB), Nonlinear Physical Chemistry Unit, Faculté des Sciences, CP231, 1050 Brussels, Belgium. mbudroni@ulb.ac.be

†Université libre de Bruxelles (ULB), Nonlinear Physical Chemistry Unit, Faculté des Sciences, CP231, 1050 Brussels, Belgium.

‡Université libre de Bruxelles (ULB), Nonlinear Physical Chemistry Unit, Faculté des Sciences, CP231, 1050 Brussels, Belgium.adewit@ulb.ac.be

and undergoes a hydrolysis reaction and (*ii*) gaseous CO_2 dissolving into an aqueous solution of NaOH. We show that the same reaction type can induce a different response on the convective dynamics depending on the reactant in the host phase. The efficiency of convective dissolution in partially miscible systems can hence be controlled by the chemicals present in the host fluid and their concentration. The direct comparison between the convective dynamics observed during CO_2 dissolution in an aqueous phase and in the ester/water stratification validates the latter as a convenient liquid-liquid model system for the interpretation of the impact of chemical reactivity in geological CO_2 sequestration.

1 Introduction

Convection represents one of the most efficient natural mechanism for mass and heat transport. A buoyancy-driven convective Rayleigh-Taylor instability can spontaneously occur when a denser fluid overlies a less dense one in the gravitational field [1] leading to a fingered deformation of an initially horizontal interface between two stratified fluids. Convective patterns can also develop in time in initially statically stable stratifications because of differential diffusion effects when the top and bottom layers involve solutes with different diffusivity [1–3] or cross-diffusive feedback. [4–6]

Currently one challenging objective is developing control strategies of such convective phenomena in problems with applied relevance. In this regard, chemical reactivity features a powerful means to impact convective dynamics by affecting *in-situ* the composition of the solutions which, in turn, can change locally a physical property of the fluids. [7–13] The capacity of chemical reactions to affect and control buoyancy-driven hydrodynamic instabilities has been demonstrated in miscible, [7–9] immiscible [10,14,15] and, more recently, in the wide class of partially miscible systems. [11,12,16,17] Convection can develop in such partially miscible systems when a buoyantly unstable density stratification forms in time along the gravity field upon dissolution with a finite solubility of one phase in the other one giving rise to buoyancy-driven fingering.

Understanding to which extent chemical processes influence the hydrodynamic stability of partially miscible stratifications is of paramount importance, as dissolution-

driven convection can be encountered in many practical issues such as CO_2 sequestration.[18–20] New promising techniques for CO_2 storage in soils involve its injection as a supercritical fluid into depleted oil fields or saline aquifers.[21–25] There, the injected less dense supercritical CO_2 first rises to an impermeable cap rock after which it starts dissolving into the partially miscible oil or salted water below it. The time needed for the fixation of the CO_2 (e.g. carbonation[26,27] or chemisorption in micro and mesoporous materials[28]) and/or for dissolution of the supercritical CO_2 into the reservoir are critical factors for its effective and safe trapping. In the latter context, convective flows in the host phase can greatly enhance the dissolution flux and it is of interest to understand how the chemical composition of the host reservoir might affect this convection. Given the difficulty to investigate these fundamental aspects *in-situ* in soils, there is a current need to (*i*) explore in laboratory-scale CO_2/water stratifications or other suitable model systems how the presence of chemical reactions can change the dynamics of convective dissolution and, possibly, enhance convective trapping and (*ii*) test theoretical predictions by comparison with these laboratory-scale data.

Nonreactive miscible two-layer stratifications with nonideal mixing properties have been proposed as simple liquid-liquid model systems to mimic supercritical CO_2 dynamics at the interface with aquifers.[29,30] Typically hydrodynamic instabilities around miscible methanol and ethylene glycol (MEG)/water or water/propylene glycol (PPG) stratifications have been studied in vertical Hele-Shaw cells.[31] Convective fingering occurs upon mixing because of a local increase of density across the initially horizontal miscible interface due to non-ideal mixing effects. Even though these model systems have been used to interpret the phenomenology of CO_2 convective dissolution, their mathematical description is different than the one of partially miscible CO_2/water double-layer stratifications, in which one phase dissolves into an other one with a finite solubility.[12,32–35] The dissolution kinetics, indeed, sustains an unstable monotonic density distribution along the gravity field due to a fixed constant concentration of the dissolving species at the fluid-fluid interface rather than a non-monotonic density profile as in miscible non-ideal mixing.[35] Also, model systems based on non-ideal mixing cannot account for the active role played by chemical processes in the convective mech-

anism.

In the search for a reliable liquid-liquid partially miscible model system, Budroni *et al.* have studied both experimentally and numerically the convective dissolution of a liquid ester into a lower denser aqueous phase as a model system for reactive partially miscible stratifications.[11] The partially miscible liquid-liquid ester/water interface is easier to handle than a gas-liquid system to approach the conditions of geologic CO_2 sequestration, where a supercritical fluid redissolves into brine. It has been shown how the reaction of the dissolved ester with a base in the water phase delays the onset of convection but also slows down the fingering growth, even inducing in some cases the formation of buoyantly stable stratifications. In parallel, other experiments involving gaseous CO_2 on top of an alkaline aqueous solution[12,17] have evidenced that a reaction can enhance and accelerate hydrodynamic fingering in partially miscible systems and that the intensity of convection depends on the concentration of the dissolved reactant present in the host phase.

These stabilising or destabilising effects depending on the nature and amount of reactants can be rationalized thanks to a general classification of the influence of A+B$\rightarrow$C chemical reactions on convective dissolution recently developed by Loodts *et al.*[12,16] It has been shown that the reaction of dissolving A with a reactant B initially dissolved in the host phase to give a product C in the solution can affect the convective dissolution because it modifies *in-situ* the density profile in the host solvent. The key point for discriminating whether the reaction has a stabilizing or destabilizing effect on convection resides in the relative contribution of the reaction product C and reactant B to density.[11,12] Provided that B and C have a comparable diffusivity, a non-monotonic density profile with a minimum builds up in time along the gravitational field if C has a solutal contribution to buoyancy forces sufficiently lower than that of the reactant B. In this case, the reaction inhibits convection as demonstrated experimentally on an ester/water example.[11] *Vice versa*, density profiles remain monotonically decreasing along the vertical with enhanced convection when the product C is sufficiently denser than the reactant B as verified experimentally using a gaseous CO_2/alkaline solution stratification.[12,17] On the basis of a linear stability analysis (LSA), the transition be-

tween these two possible cases was quantified in terms of the solutal Rayleigh numbers of the problem,[12] which measure the solutal contribution to density of the species involved in the reaction. A parametric analysis indicates that a reaction has a destabilizing effect if the Rayleigh number R_C of the product is larger than $R_B + \Delta_R$ where R_B is the Rayleigh number of reactant B and Δ_R a characteristic additional contribution quantifying the fact that C has to counterweight not only B but also part of A to change the dynamics with regard to the non reactive case. Another important parameter is the ratio β of initial concentrations of the reactants: the larger β, the larger the influence of chemistry on the convective dynamics.

To sum up, this general theoretical classification [12,16] has been validated experimentally in two cases only: the liquid/liquid ester/water system where a chemical reaction between the dissolving ester and NaOH has a stabilising influence on the fingering instability,[11] and the gaseous/liquid CO_2/water system where, on the contrary, a reaction of CO_2 with an alkaline base in solution destabilizes the system.[12,17] Up to now, there is no example of a same partially miscible system able to feature both destabilizing and stabilizing scenarios depending on the nature of the reactant B present in the host phase.

In this context, we test here both stabilising and destabilising effects of chemical reactions on convective dissolution by combined numerical and experimental work. First, we perform nonlinear simulations of reaction-diffusion-convection equations describing reactive convective dissolution of a less dense phase of A, layered on top of a reactive denser solution of B in which A is partially miscible with a constant solubility. We discuss the possible enhancement or slow down of convective processes induced by a reaction and its influence on the convective patterns. The nonlinear dynamics are compared to theoretical predictions [12,16] concerning the onset time and the characteristic wavelength of the fingered patterns as a function of $R_B - R_C$ and β. Second, we show experimentally that a same system (i.e. a two layer liquid-liquid ester/water stratification here) can be either stabilized or destabilized depending on the reactant introduced in the host phase. Third, we compare experimentally the phenomenology of the reactive convective dissolution in both the ester/water and the CO_2/water systems.

We show strong similarities between both partially miscible systems, which confirms that the reactive ester/water system is a convenient and reliable liquid/liquid model system to study supercritical CO_2 convective mixing in given host phases.

The paper is organized as follows: in section 2 we describe the physical problem, the related mathematical modeling and introduce the important parameters used to probe the convective instability. In section 3 we describe representative convective dynamics of stabilizing and destabilizing scenarios obtained from numerical nonlinear simulations and show how they support LSA results.[12,16] Convective patterns are characterized in terms of the parameters of the theory. In section 4 we compare the hydrodynamic instabilities obtained by means of two different experimental model systems (liquid/liquid ester/water or gas/liquid CO_2/water stratification) with the results from the nonlinear simulations and the general theory. Conclusions are drawn in section 5.

2 Modeling

2.1 RDC equations

We consider a two-dimensional vertical slab in a reference frame (y,z), in which z points downwards and y is the horizontal axis (Fig.1). Two partially miscible phases are in contact along a horizontal flat interface at $z = 0$ in an initially statically stable stratification (see the sketch in Fig.1.a). The upper phase A is layered over the denser phase B. We suppose that there is a local equilibrium between both phases, so that the phase A dissolves instantaneously into the lower phase B with a finite solubility A_0, which can be computed from the partitioning law of the system under study. In the lower phase, the reactant B is present in initial concentration B_0. After dissolution, A and B undergo the reaction A+B$\rightarrow$C, which takes place in the host phase, below the two-phase interface. We consider B and C insoluble in the pure phase A and we therefore focus our description of the dynamics in the host phase only where the convective instability is expected to develop. We also assume that the volume of phase A does not change significantly with the dissolution of A (at least on the characteristic hydrodynamic time scale of the experiment) and that thermal effects are negligible.[36] The

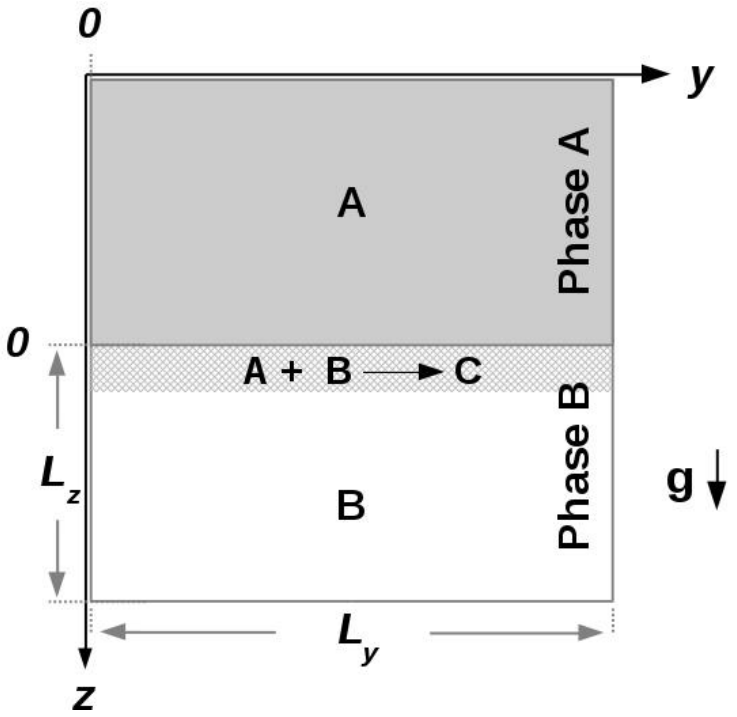

Figure 1: Schematic of the two-dimensional system considered.

spatio-temporal dynamics of this system obeys a set of partial differential equations in which the chemical kinetics is coupled to fickian diffusion and to natural convection described by Stoke's equations. Following previous modeling,[8,11,12,16,37,38] the dimensional form of the resulting Reaction-Diffusion-Convection (RDC) system reads

$$\partial_t A + (\mathbf{u}\cdot\nabla)A = D_A\nabla^2 A - qAB, \tag{1}$$

$$\partial_t B + (\mathbf{u}\cdot\nabla)B = D_B\nabla^2 B - qAB, \tag{2}$$

$$\partial_t C + (\mathbf{u}\cdot\nabla)C = D_C\nabla^2 C + qAB, \tag{3}$$

$$\nabla p = \mu\nabla^2\mathbf{u} - \rho(A,B,C)\mathbf{g}, \tag{4}$$

$$\nabla\cdot\mathbf{u} = 0\,. \tag{5}$$

Hydrodynamic equations are derived in the Boussinesq approximation, assuming that density changes only affect the gravitational term $\rho(A,B,C)\mathbf{g}$ of equation (4). $\mathbf{u} = (u,v)^T$ is the velocity field and P is the pressure. The dynamic viscosity μ, molec-

ular diffusion coefficients D_J, kinetic constant q and acceleration due to gravity $g = |\boldsymbol{g}|$ are assumed constant. Since we are interested in hydrodynamic scenarios driven by Rayleigh-Taylor-type instabilities, we set $D_A = D_B = D_C = D$ in order to avoid the concurrence of double-diffusive effects.[2,3,8]

The solutions are considered diluted so that the density of the solution can be expressed as a linear function of the concentration fields $A(y,z)$, $B(y,z)$, $C(y,z)$, according to the state equation:

$$\rho(A,B,C) \quad = \quad \rho_0(1+\alpha_A A+\alpha_B B+\alpha_C C)\,, \tag{6}$$

where ρ_0 is the density of the solvent of the lower phase, and $\alpha_J = \frac{1}{\rho_0}\frac{\partial \rho}{\partial J}$ is the solutal expansion coefficient of the J-th species with concentration J.

We introduce the set of scaled variables $\{\tilde{t} = t/t_c,\ (\tilde{y},\tilde{z}) = (y,z)/l_c,\ (\tilde{A},\tilde{B},\tilde{C}) = (A,B,C)/A_0,\ \tilde{\mathbf{u}} = \mathbf{u}/u_c,\ \tilde{\nabla}\tilde{p} = \tilde{\nabla}p/p_c - \rho_0 l_c g/p_c,\ t_c = 1/(qA_0)$ is the reaction time scale, $l_c = \sqrt{Dt_c}$ is the reaction–diffusion characteristic length and $u_c = l_c/t_c = \sqrt{D/t_c}$, $p_c = \frac{\mu}{t_c}$ and A_0 are the velocity, the pressure and the concentration scales, respectively. We also define a dimensionless density $\tilde{\rho} = (\rho - \rho_0)/\rho_c$, where $\rho_c = p_c/(l_c g)$. The model can then be written in the dimensionless form

$$\partial_t A - \partial_z\Psi\partial_y A + \partial_y\Psi\partial_z A \quad = \quad \nabla^2 A - AB\,, \tag{7}$$

$$\partial_t B - \partial_z\Psi\partial_y B + \partial_y\Psi\partial_z B \quad = \quad \nabla^2 B - AB\,, \tag{8}$$

$$\partial_t C - \partial_z\Psi\partial_y C + \partial_y\Psi\partial_z C \quad = \quad \nabla^2 C + AB\,, \tag{9}$$

$$\nabla^2\omega \quad = \quad R_A\,\partial_y A + R_B\,\partial_y B + R_C\,\partial_y C\,, \tag{10}$$

$$\nabla^2\Psi \quad = \quad -\omega \tag{11}$$

where, for convenience, the tildes have been dropped and the stream-function, Ψ, and vorticity, ω, related to the velocity field through $u = -\partial_z\Psi$, $v = \partial_y\Psi$ and $\omega = \nabla\times\mathbf{u}$

have been introduced.

The solutal Rayleigh number of the J–th species, R_J, is defined as[8,15]

$$R_J = \frac{\alpha_J A_0 g l_c^3}{\nu D} \tag{12}$$

where $\nu = \mu/\rho_0$ is the kinematic viscosity of the solvent of the bottom phase. These Rayleigh numbers quantify the solutal contribution of each chemical species to buoyancy-driven flows, as they relate the dimensionless density of the solution with the concentration fields according to

$$\rho(A,B,C) = R_A A + R_B B + R_C C. \tag{13}$$

Equations (7–11) are solved numerically by using the Alternating Direction Implicit Method (ADI) proposed by Peaceman and Rachford.[8,39] In our simulations we focus on the bottom layer of the spatial geometry sketched in Fig. 1.a and consider a rectangular domain of dimensionless width $L_y = 400$ and height $L_z = 200$, discretized over a grid of 800×400 points (i.e. we use an integration space step $h_y = h_z = 0.5$). We apply no-flux boundary conditions for all the concentration fields of the chemical species at the boundaries of the simulation domain, except for A at the top interface $z = 0$ where we take a constant value $A = 1$ that mimics the constant dimensionless concentration of this species fed from the upper phase and controlled by the partition constant. No–slip conditions are required at rigid walls for the velocty field[8] (i.e. $\Psi = 0$). The initial conditions for our simulations are: $\forall\, y : (A,B,C,\Psi) = (1,\beta,0,0)$ at the upper boundary ($z = 0$) while $(A,B,C,\Psi) = (0,\beta,0,0)$ in the remaining spatial domain, where

$$\beta = B_0/A_0 \tag{14}$$

is the ratio of initial reactant concentrations. Simulations are run using the integration time step $h_t = 1 \times 10^{-3}$.

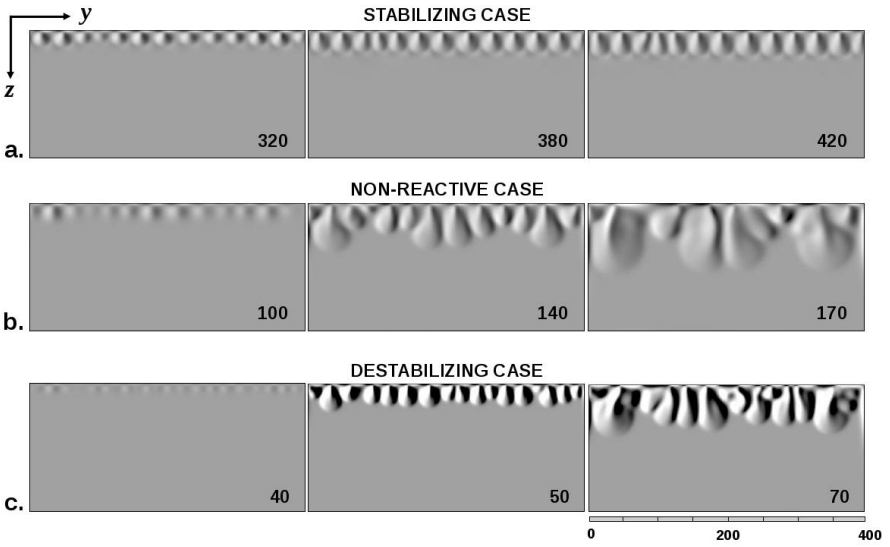

Figure 2: Spatio-temporal evolution of vorticity, $\omega(y,z,t)$, during convective fingering below the interface between two partially miscible phases. From top to bottom, typical examples of stabilizing ($R_B = 2$, $\beta = 1$), nonreactive ($\beta = 0$) and destabilizing ($R_B = -1$, $\beta = 1$) scenarios. $\omega(y,z,t)$ ranges between -0.8 (dark areas) and 0.8 (bright areas) and time of snapshot is given in the lower right corner.

3 Nonlinear simulations

The influence of reactive processes on convective dissolution has been classified theoretically in terms of the Rayleigh numbers (see Fig. 11 and Table I of[16] for a summary of currently available experiments). The intensity of the stabilizing/destabilizing effect is controlled by the amount of the solute B in the host fluid (i.e. β).[12,16]

We perform nonlinear simulations to study the impact of such changes in the spatio-temporal properties of the convective instability in the transition from the stabilizing to the destabilizing regimes by varying R_B, with $R_A = R_C = 1$. We first show representative examples of the three main cases (stabilizing ($R_B = 2$), destabilizing ($R_B = -1$) and nonreactive ($\beta = 0$)). As a second step we explore the response of the convective dynamics in terms of the characteristic onset time and wavelength of the instability for $R_B \in [-1,2]$. In order to check the influence of the initial chemical composition in the host phase, we run each numerical experiment for $\beta = 0.5$, $\beta = 1$ and $\beta = 2$.

3.1 Phenomenology

An overview of the three scenarios is displayed in Fig.2. From top to bottom, each line follows the typical evolution of the stabilizing, the nonreactive and the destabilizing cases at three different times, by showing the vorticity over the simulation spatial domain. The impact of the chemical reaction on the dynamics can be directly appreciated from the different time scales which characterize the development of convection and, in particular, from the time needed for the onset of the fingering instability. While in the stabilizing case convective fingers appear after the diffusive regime at ~ 300 time units, they become visible at ~ 90 and 40 time units in the nonreactive and destabilizing cases, respectively. The morphology and the growth rate of the fingers is also different in the three systems. As compared to the nonreactive case, the destabilizing scenario shows a more vigorous fingering characterized by a shorter wavelength at onset and convective patterns markedly elongated along the gravity field, whereas they grow slowly along the vertical direction and develop also laterally in the stabilizing example.

3.2 Characterization

For a first comparison of the dynamical properties of the reactive and nonreactive systems, we characterize the dynamics displayed in Fig.2 by following the temporal evolution of the mixing length which measures the vertical extension of the convective zone. The slope of the mixing length versus time gives an estimation of the corresponding fingering growth rate, σ. Because the development of convection is appreciated differently by looking at the velocity and the chemical fields, we compute two different mixing lengths, L_ω and L. L_ω is based on the second moment of the transversely averaged vorticity profile $\omega(y,z,t)$:

$$\langle\omega\rangle(z,t) = \frac{1}{L_y}\int_0^{L_y} \omega(y,z,t)\, dy\,. \tag{15}$$

Starting from the top border, the mixing length gives the position $L_\omega(t)$ downwards the z-axis in front of which the second moment of $\langle\omega\rangle(z,t)$ is less than 0.001. We

consider the second moment of $\langle\omega\rangle(z,t)$ to sharpen the profile shape, thus rendering the detection of mixing length extent easier. Similarly, as a comparative observable, we consider the transversely averaged profile of $A(y,z,t)$ and assume as the finger tip position $L(t)$ the point beyond which $\langle A\rangle(z,t)$ is less than 0.01. While $L_\omega(t)$ curves start with the onset of the convective instability, $L(t)$ allows us to describe the system dynamics also in the initial diffusive transient in which $L(t)$ scales as $t^{1/2}$, while $\langle\omega\rangle(z,t)$ is still negligible. On the other hand, $L_\omega(t)$ provides complementary and detailed information on the evolution of the velocity field. The results coming out from the two definitions are shown in Fig.3. The trends described with blue triangles track the destabilizing case. As compared to the nonreactive case (green squares), fingering starts earlier and follows a linear growth with a slightly larger growth rate ($\sigma \sim 1.75$ vs $\sigma \sim 1.12$). The stabilizing scenario (represented with red circles) is sharply separated from the other two cases, both in terms of onset time of the convective regime and growth rate. In this case, finger nucleation is delayed and their development follows a decreasing double-speed growth (this detail is appreciable in panel (a.) only) rather than the constant linear trend exhibited by both the nonreactive and destabilizing systems. The discontinuity in the growth rate observed in this stabilizing scenario can be related to the dynamical formation of the density minimum below the interface, which takes time to develop and decreases the finger speed by promoting lateral flows rather than a vertical growth. Thanks to $L_\omega(t)$ we can detect the onset of instability and its smooth linear growths, which cannot easily be revealed in the apparent square-root like trend of $L(t)$. Indeed the reaction refrains the fingering development such that $L(t)$ does not depart evidently from the diffusive regime. Nevertheless, perusal of Fig. 3.b shows that, starting from 320 s, $L(t)$ follows the same linear growth described by $L_\omega(t)$. In the convective regimes, σ obtained from $L_\omega(t)$ is also consistent with that of $L(t)$ for all scenarios.

3.3 Parametric classification

A systematic exploration of the transition from stabilizing to destabilizing conditions controlled by the chemical reaction has been carried out by studying the onset time

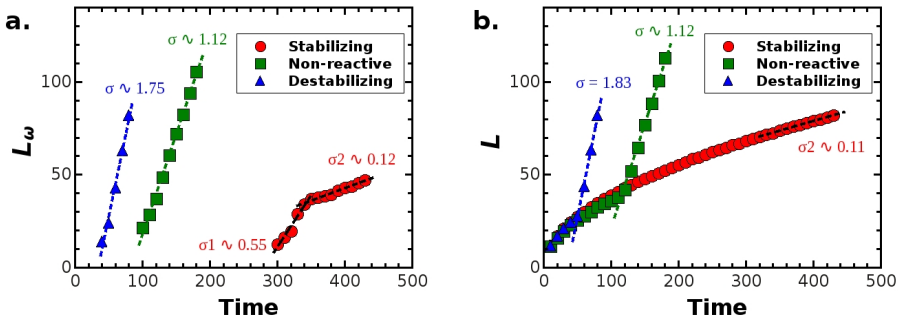

Figure 3: Mixing lengths, L_ω and L, as a function of the time for the instability scenarios shown in Fig. 2. The destabilizing, nonreactive and stabilizing case are indicated with triangles, squares and circles, respectively. The growth rates, σ, are estimated by the linear regression of $L_\omega(t)$ and $L(t)$ in the linear regime.

t^* (computed as the time at which $|\omega(y,z,t)|$ becomes larger than 0.1 and the velocity field effectively modifies the chemical fields) as a function of R_B, keeping R_A and R_C fixed to 1. This allows to compare the results of our nonlinear simulations with the characteristic trends and the general classification provided by Loodts et al. [12,16] Following this formalism, we analyze the dependence of t^* upon the difference $R_B - R_C$, spanning the range $[-2,1]$ (i.e. we vary $R_B \in [-1,2]$). The green, the grey and the red curves in Fig.4.a illustrate the instability onset time when the initial concentration ratio $\beta = 2$, $\beta = 1$ and $\beta = 0.5$, respectively. In general, t^* follows a sigmoid profile, monotonically increasing with $R_B - R_C$. As predicted in the general theory, [12,16] there is a threshold Δ_R (here ~ 0.5) beyond which t^* of the reactive systems is larger than that of the nonreactive analog, represented by the black dotted line at $t^* \sim 90$. On the basis of this property, Fig.4.a is divided in the destabilizing ($R_B - R_C < -\Delta_R$) and the stabilizing domain ($R_B - R_C > -\Delta_R$). All the curves for different β intersect the nonreactive value close to $-\Delta_R$, confirming that the value of this latter quantity only slightly changes with β. [12,16] On the other hand, the stabilizing or destabilizing effect of the reaction intimately depends on β and, in particular, the reactive t^* increasingly departs from the non reactive value when β increases (implying increasing B_0). The green, the grey and the red curves show progressively that, by increasing β, the fingering instability sets in faster in the destabilizing region whilst it is delayed in the stabilizing

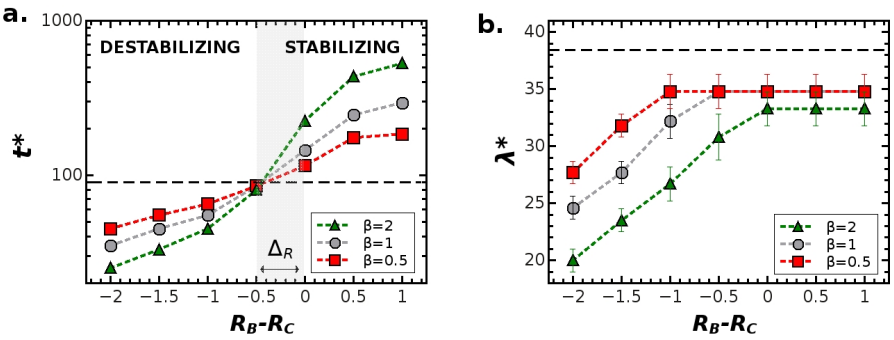

Figure 4: Instability onset time, t^* (a), and convective pattern wavelength, λ^* (b) as a function of $(R_B - R_C)$. The red curves describe the case $\beta = 0.5$ while the grey and the green curves characterize $\beta = 1$ and 2, respectively. The black dashed line corresponds to the nonreactive reference.

domain. The trends of t^* measured in our nonlinear simulations compare favourably with those predicted by Loodts *et al.*[12]

The characteristic wavelength λ^* of the convective patterns is quantified as a function of $R_B - R_C$ in Fig. 4.b for $\beta = 0.5$, 1 and 2. The dominating mode (and the corresponding λ^*) characterizing the instability has been calculated from the fast Fourier transform of the transverse profile of the vorticity along the top border of the spatial domain at onset time, t^*. Both reactive systems have a shorter wavelength than the nonreactive case (this is consistent with[12,16]). Though this feature is not surprising for the destabilizing case, it is somewhat counter-intuitive in the stabilizing scenario. Convective patterns also present shorter λ^* by increasing β in the destabilizing domain, while all trends converge to a plateau for $(R_B - R_C) > -\Delta_R$.

In agreement with the results of previous theoretical work,[12,16] nonlinear simulations indicate that the efficiency of the convective dissolution in reactive systems not only depends on the relative contribution to the global density of reactants and products (*via* the Rayleigh numbers), but also on the amount of the initial reactant in the host layer *via* β. Increasing β amplifies the influence of a chemical process as further confirmed by experimental evidences below.

4 Comparison with experiments

To further analyse the impact of reactions on convective dissolution, let us now turn to experimental studies starting with a liquid-liquid ester/water partially miscible stratification where a switch from the stabilizing to the destabilizing case can be induced by changing the chemical environment in the water phase.

4.1 Experimental setup

We study the stratification of ethyl-formate/aqueous-solution in the gravitational field in a quasi-two-dimensional cell, where the less dense pure liquid ester phase is set on top of the aqueous layer. The experimental set-up consists of a vertically oriented Hele-Shaw cell of dimension 3.5 cm $\times$ 7 cm, made of two borosilicate glass plates separated by a thin polymer mask giving a gap width of 0.5 mm (see[4,8,11,40]). The two liquids are simultaneously pumped into the cell, by means of two independent plastic syringes through two inlets positioned at the top and bottom of the reactor. The shape of the polymer mask favors the exhaustion of the excess of the liquids through the cell's outlets located at the lateral sides of the reactor, until a flat interface between the two liquids is obtained. Both the cell inlets and outlets are finally closed to avoid leakage. The dynamics is monitored by using a phase-shift schlieren technique which allows to track the variations in space and time of the refractive index, related to the density variations inside the system. With this technique we can avoid the introduction of dyes and their related artificial effects on the global dynamics.[41–43] All reactants are commercial grade reactants (Sigma-Aldrich) used without further purification. The ester phase consists of pure ethyl-formate (97%) while stock aqueous solutions with different concentration of formic acid, HCOOH, and sodium hydroxide, NaOH, are prepared using deionized water. All experiments have been performed at 20 °C.

4.2 Alkyl-formate dissolution in water phase

Alkyl-formates are organic compounds with general formula HCOOR′ where R′ is an alkyl chain. They are partial miscible in water, with a decreasing tendency to mix as the length of the alkyl chain is augmented. The formates undergo hydrolysis yielding formic acid and the alcohol R′OH according to the kinetic scheme

$$\mathrm{HCOOR'} + \mathrm{H_2O} \underset{\mathrm{k_{-1}}}{\overset{\mathrm{k_1}}{\rightleftharpoons}} \mathrm{HCOOH} + \mathrm{R'OH}\,. \tag{16}$$

The process occurs either in neutral, acid and basic conditions and is slightly endothermic.[44] As it is well-known from the previous literature,[44] the kinetics of the process is autocatalytic when it is carried out in an acidic environment i.e.

$$\mathrm{HCOOR'} + \mathrm{H_2O} \underset{\mathrm{k_{-a}}}{\overset{\mathrm{H^+,k_a}}{\rightleftharpoons}} \mathrm{HCOOH} + \mathrm{R'OH}\,, \tag{17}$$

with $k_a > k_1$ ($k_a = 2.52 \times 10^{-3}$ $\mathrm{M^{-1}\ s^{-1}}$ see[45]). In neutral conditions, the evolution of the reaction follows the initial non-autocatalytic path (16) and then switches to the competing autocatalytic mechanism (17) when a sufficient concentration in acid is reached (HCOOH is a relatively strong acid with a pK_a = 3.751 at 25 °C). In general, in neutral conditions, the process is very slow (the pseudo-first order rate constant k_1 ranges between 10^{-7} and 10^{-5} $\mathrm{s^{-1}}$ for simple formates (R′ = -$\mathrm{CH_3}$, -$\mathrm{C_2H_5}$, -$\mathrm{C_3H_7}$)[46] at 25 °C) and can be considered negligible.

By contrast, the reaction is significantly accelerated in alkaline conditions where it takes place *via* a S_N2 mechanism.[47] Apart for the alcohol, the product of the alkyl-formate hydrolysis in an alkaline solution is the formate salt HCOOM associated with the base MOH, according to the second order kinetics

$$\mathrm{HCOOR'} + \mathrm{MOH} \underset{\mathrm{k_{-b}}}{\overset{\mathrm{k_b}}{\rightleftharpoons}} \mathrm{HCOOM} + \mathrm{R'OH}\,, \tag{18}$$

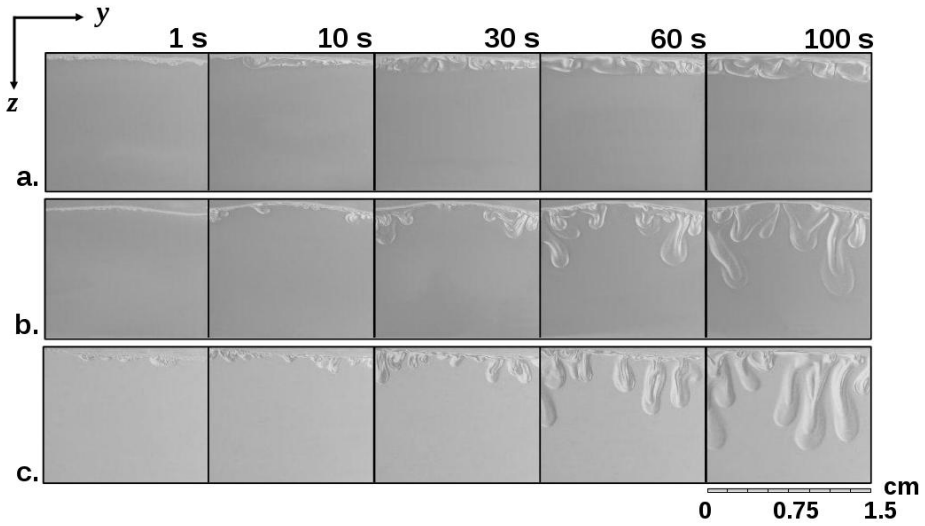

Figure 5: Convective dissolution of the ethyl-formate in the aqueous phase. From top to bottom, experiments with (a.) a solution [NaOH] = 0.25 M (stabilizing case), (b.) pure water (nonreactive case), and (c.) [HCOOH] = 0.01 M (destabilizing case). All snapshots have a field of view 1.50 cm $\times$ 1.35 cm.

where M stands for the positive counter ion of OH^-.

The ethyl-formate hydrolysis well approximates the reaction scheme A+B $\rightarrow$ C, if it is to study density-driven hydrodynamic instabilities, as the byproduct, EtOH, barely contributes to the global density (see discussion below).

4.2.1 Results

The convective instability observed experimentally in the nonreactive ethyl-formate/water stratification and the stabilizing scenario obtained with alkaline solutions have been treated in previous work.[11] However, for a complete discussion on the agreement between the theoretical classification above and the experimental system, we briefly resume hereunder the main results of both cases.

Nonreactive scenario. In Fig.5.b we show the typical nonreactive dynamics below the ester/water interface: starting from a buoyantly stable configuration in which the less dense ester phase overlies the denser pure water layer ($\rho_{HCOOEt} = 0.921$ g/cm^3 vs $\rho_{H_2O} = 0.998$ g/cm^3 at 20 °C), a hydrodynamic density fingering instability develops

below the interface upon the dissolution of the pure ethyl-formate into the water. As mentioned above, the hydrolysis process is here extremely slow with respect to the time scale at which the hydrodynamic instability occurs and, hence, this experiment is representative of nonreactive cases where convective fingering is solely triggered by the local density increase due to the mass transfer of ester from the top to the bottom phase.

In Fig.6, we track the temporal evolution of the instability by plotting the location of the finger tip, L, along the vertical axis with regard to the position of the initial contact line between the two layers. The spatio-temporal curve of the nonreactive system (averaged on 6 experiments), described with red diamonds in Fig. 6, shows that the mixing zone of fingers grows linearly in time with $\langle\sigma\rangle \sim 0.0063$ cm s^{-1}.

Stabilizing reactive scenario. When the hydrolysis process is catalyzed by the base NaOH, the chemistry of the system comes into play following the second order kinetics (18) and causes a strong stabilization of the convective instability (Fig.5.a). The onset of convective fingering is delayed as compared to the nonreactive case and fingers develop only on a much longer time scale. This is due to the fact that the sodium formate produced by the hydrolysis reaction ($\alpha_{\mathrm{HCOONa}} = 0.0410$ M^{-1}) has a smaller contribution to density than the base NaOH initially present in the host phase ($\alpha_{\mathrm{NaOH}} = 0.044$ M^{-1}, see[48]). The resulting density distribution along the gravitational axis, featuring a depletion zone below the interface, induces a stabilizing effect as it creates a lower density barrier that refrains the fingering growth.[11,12] This system presents the general characteristics of a stabilizing scenario described in the parametric classification given in[12,16] and in sec. 3. By comparing this dynamics with the nonreactive case, we can see how, due to the formation of a density depletion area below the interface, fingers not only evolve slower, but also experience a dynamical increment of the wavelength, showing transversely expanding squared patterns. The qualitative morphology of these patterns compare favourably with the convective dynamics obtained in nonlinear simulations of the stabilizing case (cfr. Fig. 2.a).

The influence of the alkaline hydrolysis on the speed of growth of the fingers has been

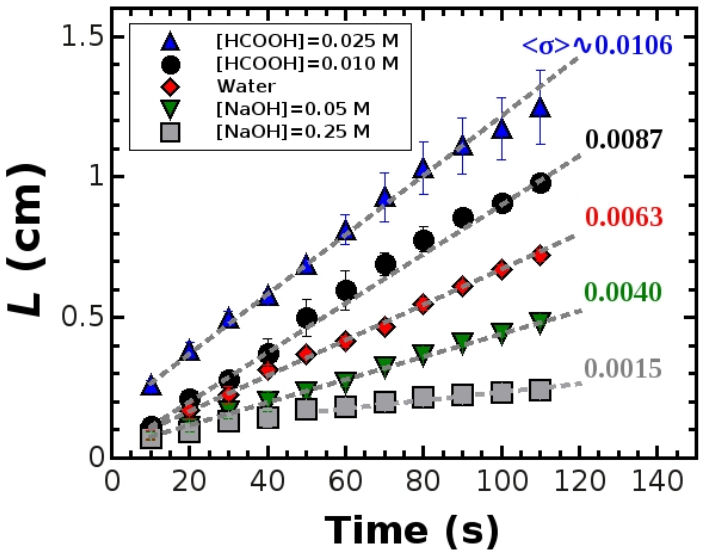

Figure 6: Spatio-temporal characterization of the fingering instability developing below the interface between pure ethyl-formate and a solution of (*i*) [NaOH]= 0.25 M (grey squares), (*ii*) [NaOH] = 0.05 M (green reversed triangles), (*iii*) pure water (red diamonds), (*iv*) [HCOOH] = 0.01 M (black circles) and (*v*) [HCOOH] = 0.025 M (blue triangles). Each curve represents the average of six experiments. The related average growth rates, $\langle\sigma\rangle$, are estimated by the linear regression of the mixing length L versus time, and are expressed in cm s^{-1}.

also studied as a function of the NaOH concentration in the aqueous layer (see also [11]). Fig.6 shows two different alkaline solutions with concentration 0.05 M (green reversed triangles) and 0.25 M (grey squares) of NaOH, where the instability growth rate decreases with the base concentration ($\langle\sigma\rangle \sim 0.0040$ cm s^{-1} for [NaOH]=0.05 M vs $\langle\sigma\rangle \sim 0.0015$ cm s^{-1} for [NaOH]=0.25 M). This is in good agreement with theory predicting that the stabilizing "power of chemistry" is enhanced when β is increased.

Destabilizing reactive scenario. A very different dynamics is obtained if the ester hydrolysis process is now catalyzed by an acid. According to the kinetic scheme (16), the acidic hydrolysis reaction self-sustains the formation of fresh formic acid and alcohol. This process promotes an increase of the density below the interface due to the conversion of the dissolving ester into the denser formic acid (α_{HCOOH} [48] = 0.011 M^{-1} while EtOH has a decreasing effect of second order $\alpha_{\mathrm{EtOH}} = -0.008$ M^{-1}). This enhances

the density maxim below the interface with respect to the nonreactive situation. Referring to the parametric taxonomy depicted in Fig.4 and in,[12,16] the reactive dissolution of the ethyl-formate in an acidic solution falls then into the category of destabilizing cases. This can be directly appreciated in Fig. 5 which provides a parallel between the typical fingering instability of the nonreactive case (b.), and that of the reactive stratification of the ester on top of an acidic solution 0.01 M of HCOOH (c.). In the latter case, as soon as a flat interface between the two layers is achieved, fingers immediately nucleate along the entire initial interface, while the development of fingers is slower and localized to the side borders of the cell in the nonreactive analogue. We can also observe how convective mixing is more intense both in terms of finger growth rate and number of fingers. This description is also consistent with nonlinear simulations for destabilizing scenarios (see Figs. 2.a, 3 and 4).

The enhanced spatio-temporal development of the convective instability in the presence of the acid is examined as a function of the acid concentration in Fig.6. Black circles and blue triangles describe the experiments performed with the solutions 0.01 M and 0.025 M of HCOOH, respectively. Both trends $L(t)$ exhibit a noticeable increment with respect to the nonreactive curve, indicating a higher growth rate $\langle\sigma\rangle$ of the instability when increasing [HCOOH]. Fig.6 also shows the impact of the acidic autocatalysis on the onset and development of the instability. When the concentration of HCOOH is low (see the curve for the case 0.01 M), the initial growth rate of the convective structures is slightly larger but comparable to that of the nonreactive system. After an induction period, the trends related to the acidic and neutral hydrolysis diverge, as the autocatalytic path of the process is effectively turned on and triggers the formation of the destabilizing formic acid. However, [HCOOH]=0.025 M is large enough to start the autocatalytic kinetics and its related influence on the convective dissolution immediately. In these conditions both the reactivity and surface tension effects at the interface are enhanced and render also difficult to achieve a sufficiently flat and narrow initial condition between the two layers. The value of the mixing length is thus initially slightly augmented and there is a clear separation between the L curve of the experiment for HCOOH = 0.025 M and that of pure water. A further increment of the

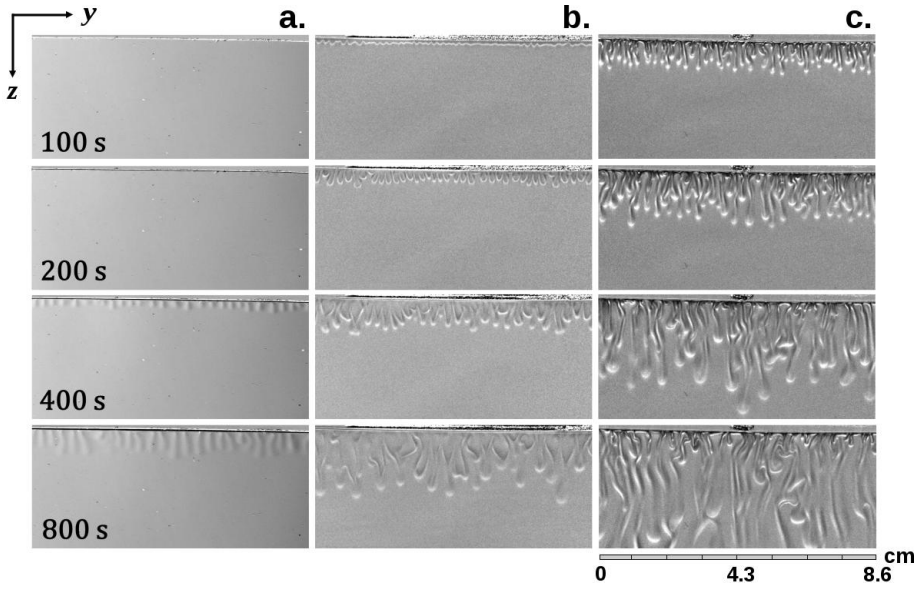

Figure 7: Development over time of the fingering instability induced by the dissolution of gaseous CO_2 in water (a.) and in reactive aqueous solutions of NaOH in concentrations of 0.01 M (b.) and 0.1 M (c.). The field of view is 8.6 cm x 3.9 cm and focuses on the lower aqueous phase where the density-driven instabilities develop. The temperature is 20°C.

acid concentration does not lead to any significant additional enhancement of the finger growth rate as the autocatalytic effect of the acid reaches a saturation.[44] Also, we observed that further increasing the acid concentration in the bottom solution induces non-negligible interfacial Marangoni contributions to the global flow, thus altering the nature of the density fingering phenomenology which is the focus of this work.

4.3 Comparison with CO_2 dissolution in water phase

An acid-base reaction has already been shown experimentally to strengthen CO_2 convective dissolution in aqueous reactive solutions.[12,49] Here we deepen this study by performing a characterization of dynamics during gaseous CO_2 dissolution in water and in aqueous NaOH solutions at different concentrations in order to show that this system behaves qualitatively like the ester/water partially miscible stratification.

The set-up for the experiments on CO_2 convective dissolution is similar to the one used for the ester/water system but is larger. Explicitly, a gas-tight vertical Hele-Shaw cell

of dimension 21 cm $\times$ 26 cm is partially filled with deionised water or with NaOH aqueous solutions of variable concentrations (0.01M, 0.02M, 0.05M and 0.1M). Pure gaseous CO_2 is injected through the top of the cell at atmospheric pressure and constant flow rate (6.0 L/h) to start the experiment. Visualization is made by a schlieren technique as well. Before each experiment, the cell is purged with N_2 to avoid premature dissolution of atmospheric CO_2 in the solution. Upon injection of CO_2 into the cell, this gas rapidly replaces N_2 and spreads homogeneously above the aqueous interface before dissolving into the aqueous phase. The dissolved CO_2 instantaneously forms the acidic H_2CO_3 which, in reactive solutions, reacts with NaOH to form Na_2CO_3, denser than both reactants. Although the detailed reactive scheme is more complex than A+B$\rightarrow$C,[17] we can roughly assume that A = CO_2 ($\alpha_A = 0.0082$ M^{-1}), B = NaOH ($\alpha_B = 0.044$ M^{-1}) and C = Na_2CO_3 ($\alpha_C = 0.105$ M^{-1}). The Rayleigh numbers for these chemical species read R_A= 0.102, R_B= 0.548 and R_C = 1.308 which thus gives $R_b - R_c$ = -0.760. Theory[12] predicts that we are typically in a destabilizing case as the product C has a larger contribution to density than A and B.

4.3.1 Results

Fig. 7a. shows the typical development of the density-driven fingering instability which develops upon dissolution of CO_2 in water, i.e. the nonreactive case. Soon after the injection of CO_2 inside the cell, a denser CO_2-enriched boundary layer starts to develop just below the interface. This layer is then readily destabilized into small fingers sinking from the interface. Over time, the fingers grow, enlarge, and penetrate more deeply into the aqueous solution with some non-linear effects like merging for example. As expected, it is seen that the fingering instability develops faster in reactive solutions (Fig. 7b. and c.) than in pure water, and convection is enhanced if the concentration of the reactant is increased (i.e. when β is increased). Furthermore, as the concentration of NaOH increases, the onset time is shorter, which is in agreement with the destabilizing trend predicted theoretically (cfr. with Fig.4.a). This effect is clearly visible in Fig.8 which quantifies the evolution of the finger growth (L) as a function of time for water and for increasing concentration of NaOH. The trends seen on Fig. 8

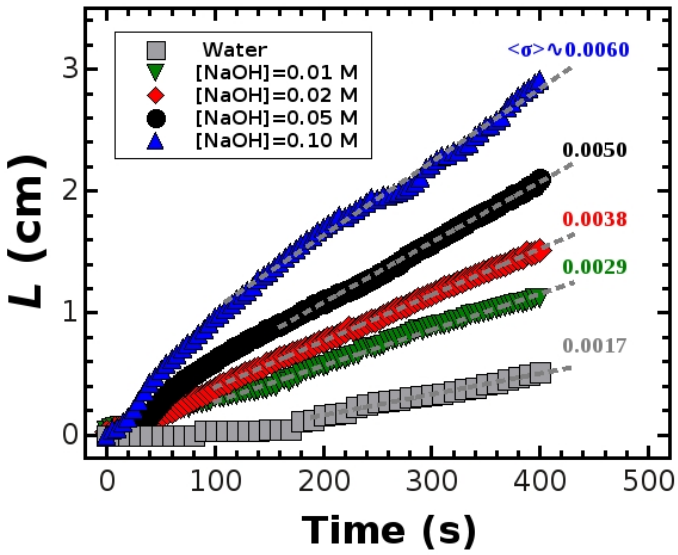

Figure 8: Spatio-temporal evolution of the finger growth characterizing the convective instability developing upon CO_2 dissolution in water and in NaOH solutions with increasing concentration. Each curve represents the average of five experiments. The average growth rates, $\langle\sigma\rangle$, are estimated by the linear regression of the mixing length L versus time, and are expressed in cm s^{-1}.

and the related growth rates confirm that varying β is a good way to control the intensity of convective dissolution in reactive systems. The destabilizing effect of chemical reactions on the development of the fingering instability in the CO_2/water system is therefore very similar to the ester/water system. This confirms that the ester/water system is a good analogue to study convective dissolution dynamics for CO_2 sequestration with an easy-to-handle liquid/liquid stratification.

5 Conclusion

Chemical reactions influence drastically the buoyancy-driven convective dynamics developing when one phase A dissolves into a partially miscible reservoir containing a solute B by affecting the density profile in the host phase. Even a simple reaction of the type A+B $\rightarrow$ C can thus enhance or refrain convective dissolution depending whether the reaction product C increases or decreases the local density with respect to the initial value. This implies that the same reaction type can induce a different effect

on the global dynamics when the reactant B in the host phase (and thus the product C forming in the mixing zone) is varied. The efficiency of convective dissolution in partially miscible systems can therefore be controlled by suitably selecting the chemicals present in the host fluid. Also, increasing the initial concentration of the reactant B plays a significant role by intensifying the effect of the reaction on convection. In line with the recent general classification on the effects of a chemical reaction on convective dissolution,[12,16] we have here studied all these fundamental features by means of experiments and nonlinear simulations of a reaction-diffusion-convection model describing the dissolution dynamics of a less dense fluid on top of a reactive denser phase. The transition from stabilizing to destabilizing scenarios has been studied numerically as a function of the relative contribution of the species B to the density (R_B), keeping R_A and R_C fixed. These nonlinear simulations confirm theoretical predictions, i.e. there exists a critical Δ_R value above which R_C is sufficiently larger that R_B to switch the system from destabilizing to stabilizing. The nonlinear dynamics also shows that tuning the chemistry and the initial concentration of B can be used to change the onset time of convection and the wavelength of the fingered pattern. The spatio-temporal dynamics and convective patterns observed in the numerical study compare favourably with experiments carried out with (*i*) an alkyl formate stratified on top of an aqueous solution giving an hydrolysis reaction after dissolution and (*ii*) gaseous CO_2 dissolving into an alkaline solution of NaOH. By using the ester/water solution system we have been able to span the transition from stabilizing to destabilizing scenarios by changing the chemical environment of the host aqueous phase from basic to acidic. Also, the ester/aqueous solution stratification allows us to show a new example of destabilizing reactive scenario. By contrast, the experiments with CO_2 have focused on destabilizing scenarios, showing that increasing the base concentration strengthens the reaction effect and enhances the fingering dynamics. A qualitative comparison between the phenomenology and the mechanism underneath the convective dissolution of the ester and CO_2 into aqueous solutions validates the former as a consistent, easy-to use laboratory-scale liquid-liquid model system on which to study fundamental questions related to CO_2 sequestration.

In the context of geologic CO_2 sequestration, the results of this study indicate that the chemical composition of a given geologic site certainly has an important impact on the efficiency of CO_2 convective dissolution. Further aspects, such as more complex kinetic schemes, differential diffusion, possible changes in the viscosity or surface-tension-driven flows will next have to be taken into account to develop a general theory for controlling and optimizing convective dissolution. A quantitative comparison between numerics and experiments requires to test case by case the assumptions of the model with "ad-hoc" studies where the parameters defining the system are evaluated and included in the modeling. This constitutes the object of our work in progress.

6 Acknowledgments

The authors thank V. Loodts, L. Rongy and V. Pimienta for fruitful discussions. M.A.B. is supported by FRS-FNRS. A.D. and C.T. acknowledge funding by PDR-FNRS FORECAST project.

References

[1] J. Fernandez, P. Kurowski, P. Petitjeans and E. Meiburg, *J. Fluid Mech.*, 2002, **451**, 239–260.

[2] P. M. J. Trevelyan, C. Almarcha and A. De Wit, *J. Fluid Mech.*, 2011, **670**, 38–65.

[3] T. Radko, *Double-diffusive convection*, Cambridge University Press, Cambridge, UK, 2013.

[4] M. A. Budroni, L. Lemaigre, A. De Wit and F. Rossi, *Phys. Chem. Chem. Phys.*, 2015, **17**, 1593–1600.

[5] M. A. Budroni, J. Carballido-Landeira, A. De Wit and F. Rossi, *Chaos*, 2015, **25**, 064502.

[6] M. A. Budroni, *Phys. Rev. E*, 2015, **92**, 063007.

[7] C. Almarcha, P. M. J. Trevelyan, P. Grosfils and A. De Wit, *Physical Review Letters*, 2010, **104**, 044501.

[8] L. Lemaigre, M. A. Budroni, L. A. Riolfo, P. Grosfils and A. De Wit, *Phys. Fluids*, 2013, **25**, 014103.

[9] D. A. Bratsun, K. Kostarev, A. Mizev and E. Mosheva, *Phys. Rev. E*, 2015, **92**, 011003.

[10] K. Eckert and A. Grahn, *Phys. Rev. Lett.*, 1999, **82**, 4436–4439.

[11] M. A. Budroni, L. A. Riolfo, L. Lemaigre, F. Rossi, M. Rustici and A. De Wit, *J. Phys. Chem. Lett.*, 2014, **5**, 875–881.

[12] V. Loodts, C. Thomas, L. Rongy and A. De Wit, *Phys. Rev. Lett.*, 2014, **113**, 114501.

[13] A. De Wit, *Phil. Trans. R. Soc. A*, 2016, **374**, 20150419.

[14] S. S. S. Cardoso and J. T. H. Andres, *Nature Communications*, 2014, **5**, 5743.

[15] I. Cherezov and S. S. S. Cardoso, *Phys. Chem. Chem. Phys.*, 2016, **18**, 23727–23736.

[16] V. Loodts, L. Rongy and A. De Wit, *Phys. Chem. Chem. Phys.*, 2015, **17**, 29814.

[17] C. Thomas, V. Loodts, L. Rongy and A. D. Wit, *International Journal of Greenhouse Gas Control*, 2016, **53**, 230 – 242.

[18] T. J. Kneafsey and K. Pruess, *Transp. Porous Med.*, 2010, **82**, 123–139.

[19] A. Riaz, M. Hesse, H. A. Tchelepi and F. M. Orr, *J. Fluid Mech.*, 2006, **548**, 87–111.

[20] V. Loodts, L. Rongy and A. De Wit, *Chaos*, 2014, **24**, 043120.

[21] K. S. Lackner, *Science*, 2003, **300**, 1677–1678.

[22] S. Pacala and R. Socolow, *Science*, 2004, **305**, 968–972.

[23] F. M. J. Orr, *Science*, 2009, **325**, 1656–1658.

[24] M. L. Szulczewski, C. W. MacMinn, H. J. Herzog and R. Juanes, *Proc. Natl. Acad. Sci. USA*, 2012, **109**, 5185–5189.

[25] IPCC, *Climate Change 2013: The Physical Science Basis. Contribution of Working Group I to the Fifth Assessment Report of the Intergovernmental Panel on Climate Change*, Cambridge University Press, Cambridge, United Kingdom and New York, NY, USA, 2013, p. 1535.

[26] G. Gadikota, J. Matter, P. Kelemen and A. A. Park, *Phys. Chem. Chem. Phys.*, 2014, **16**, 4679–4693.

[27] H. Zhao, Y. Park, D. H. Lee and A. A. Park, *Phys. Chem. Chem. Phys.*, 2013, **15**, 15185–15192.

[28] E. De Canck, I. Ascoop, A. Sayari and P. Van Der Voort, *Phys. Chem. Chem. Phys.*, 2013, **15**, 9792–9799.

[29] J. A. Neufeld, M. A. Hesse, A. Riaz, M. A. Hallworth, H. A. Tchelepi and H. E. Huppert, *Geophys. Res. Lett.*, 2010, **37**, L22404.

[30] S. Backhaus, K. Turitsyn and R. E. Ecke, *Phys. Rev. Lett.*, 2011, **106**, 104501.

[31] P. A. Tsai, K. Riesing and H. A. Stone, *Phys. Rev. E*, 2013, **87**, 011003.

[32] J. J. Hidalgo, J. Fe, L. Cueto-Felgueroso and R. Juanes, *Phys. Rev. Lett.*, 2012, **109**, 264503.

[33] M. C. Kim, *Physics of Fluids*, 2014, **26**, 114102.

[34] S. M. Jafari Raad and H. Hassanzadeh, *Phys. Rev. E*, 2015, **92**, 053023.

[35] S. M. Jafari Raad, H. Emami-Meybodi and H. Hassanzadeh, *Water Resources Research*, 2016, **52**, 4458–4468.

[36] C. Almarcha, P. M. J. Trevelyan, P. Grosfils and A. De Wit, *Phys. Rev. E*, 2013, **88**, 033009.

[37] L. Rongy, P. M. J. Trevelyan and A. De Wit, *Phys. Rev. Lett.*, 2008, **101**, 084503.

[38] L. Rongy, P. M. J. Trevelyan and A. De Wit, *Chem. Eng. Sci.*, 2010, **65**, 2382–2391.

[39] D. W. Peaceman and H. H. Rachford, *J. Soc. Ind. Appl. Math.*, 1955, **3**, 28.

[40] Y. Shi and K. Eckert, *Chem. Eng. Sci.*, 2008, **63**, 3560–3563.

[41] C. Almarcha, P. M. J. Trevelyan, L. A. Riolfo, A. Zalts, C. El Hasi, A. D'Onofrio and A. De Wit, *The Journal of Physical Chemistry Letters*, 2010, **1**, 752–757.

[42] S. Kuster, L. A. Riolfo, A. Zalts, C. El Hasi, C. Almarcha, P. M. J. Trevelyan, A. De Wit and A. D'Onofrio, *Phys. Chem. Chem. Phys.*, 2011, **13**, 17295–17303.

[43] C. Thomas, L. Lemaigre, A. Zalts, A. D'Onofrio and A. De Wit, *Int. J. Greenh. Gas Con.*, 2015, **42**, 525–533.

[44] O. Jogunola, T. Salmi, K. Eranen, J. Warna, M. Kangas and J. P. Mikkola, *Ind. Eng. Chem. Res.*, 2010, **49**, 4099–4106.

[45] S. Begum, *Journal of the Chemical Society of Pakistan*, 2001, **23**, 139–143.

[46] S. Begum, M. Zeb and N. Pizada, *Journal of the Chemical Society of Pakistan*, 2000, **22**, 255–259.

[47] S. Patai, *The Chemistry of Carboxylic Acids and Esters*, John Wiley and Sons Ltd: Chichester, New York, Brisbane, Toronto, 1969.

[48] W. M. Haynes, D. R. Lide and T. J. Bruno, *CRC Handbook of Chemistry and Physics 2012-2013*, CRC Press, 2012.

[49] C. Wylock, B. Haut, A. Rednikov and P. Colinet, *The Journal of Physical Chemistry B*, 2014, **118**, 11323–11329.